XMM-Newton: a pathfinder for future multi-wavelength and multi-messenger observations with Athena

This project has received funding from the European Union's Horizon 2020 research and innovation programme under Grant Agreement No. 101004168.

Work Package WP6

Spectra

Deliverable D6.1

Fitting products for extracted spectra

Due date:	31.11.2021
Nature[1]:	R
Dissemination Level[2]:	PU
Work Package:	Spectra
Lead Beneficiary:	University of Cantabria
Contributing Beneficiaries:	MPG/MPE, CEA
Version:	4

1 **Nature:** **R** = Report, **P** = Prototype, **D** = Demonstrator, **O** = Other

2 **Dissemination level** **PU** = Public
PP = Restricted to other programme participants (including the Commission Services)
RE = Restricted to a group specified by the consortium (including the Commission Services)
CO = Confidential, only for members of the consortium (including the Commission Services)
Restraint UE = Classified with the classification level "Restraint UE" according to Commission Deci-sion 2001/844 and amendments
Confidential UE = Classified with the mention of the classification level "Confidential UE" according to Commission Decision 2001/844 and amendments
Secret UE = Classified with the mention of the classification level "Secret UE" according to Commis-sion Decision 2001/844 and amendments

Table of Content

1 Introduction

This report is about the first deliverable of work package six (D6.1) of the EU funded XMM2Athena project, where we fitted an absorbed power law model to all extracted spectra in the 4XMM–DR11 catalogue. We provide best fit parameter values and confidence intervals. We took all the detections in the 4XMM–DR11 catalogue into account and tried to fit their spectra. Of course, we could not achieve a good fit for all these detections. All issues that we encountered during the fitting are described below and flagged in the catalogue.

2 Data and analysis

The 4XMM–DR11 catalogue contains 319565 detections with spectra in 11907 observations. There are 100237 (31.4 per cent) detections that are made in both detectors, 145342 (45.5 per cent) detections that come solely from the pn detector and 73986 (23.2 per cent) detections that are only from the MOS cameras.

To reduce the run time of the spectral fits we merged all spectra of the same detection in the same observation for the same instrument using the SAS task *epicspeccombine*. This means that we end up with at most one pn and one MOS spectrum for each detection. Detections where the background spectrum of at least one detector has zero counts and detections where the net counts in at least one detector are less than zero are excluded from our spectral analysis (see Sect. 3). The distributions of background and net counts in the spectra (after merging) for the *Good sample* (see Sect. 3 and Table 1) are shown in Fig. 1.

2.1 Fitting

We used python scripts to perform the automated fits making use of the fitting and modelling software Sherpa 4.9.1 [Freeman et al., 2001] and the analysis software BXA [Bayesian X-ray Analysis; Buchner et al., 2014]. We binned the spectra to have at least 1 count per bin. To preserve Poisson statistics the source and background spectra would need to be modelled simultaneously. Actually, the fitting is performed in a two-step process. In the first step we fitted the merged background spectra with an empirical background model (see Sect.2.2.1) and saved the best fit parameters. The fitting of the source + background spectra with fixed best-fit background parameters is done in the second step.

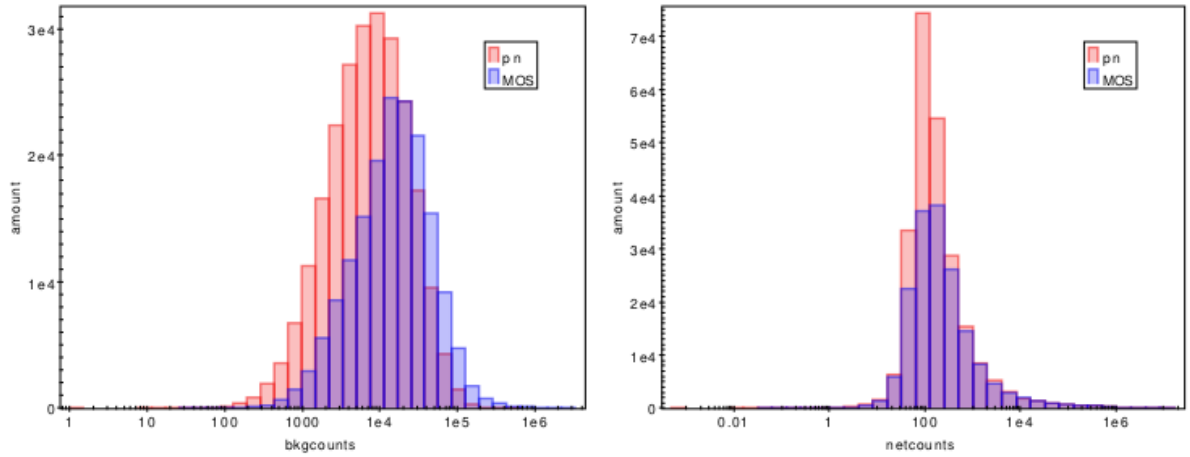

Figure 1: Distribution of background counts (left panel) and net counts (right panel; after merging the spectra of the same detection in the same observation for the same instrument) of the Good sample in the 0.2 – 12.0 keV band.

2.2 Spectral models

2.2.1 Background model

As background model we used the XMM-Newton empirical background model developed by Richard Sturm at MPE [Maggi et al., 2014], which is part of the bxa.sherpa.background module. This model consists of a part that accounts for emission of the cosmic X-ray background and X-ray emission of the local hot bubble and Galactic halo. In addition, it includes a part that models the detector background and contains the contribution of lines. This part is not folded through the instrumental response.

The background model, which is made up of a mixture of power laws, Gaussian lines and thermal emission components, is fitted in a multi-step process to the background spectrum with an increasing complexity of the model in each step, and with the parameters of the previous steps constrained within a narrow range of the best-fit value obtained in the previous step. With this stepwise approach and thanks to the high number of background counts for most of the observations (see left panel of Fig. 1) the many free parameters of this model give us acceptable fits. Nevertheless, we did some tests with a simplified version of the background model, reducing the number of free parameters, and found that the parameters of the source model (obtained with the different sets of background parameters) agree within errors and most of them follow a one-to-one correlation closely. Thus, we conclude that the empirical background model within BXA gives an acceptable description of the background and does not introduce any distortion in the source parameters.

To estimate the goodness of fit of the background spectra we use a χ^2 test. Therefore, we need to obtain in a first step the number of effective parameters for pn and MOS, since not all background model components are needed for all background spectra. We obtained χ^2 values for all detections in XMM-DR10 with 1000 background counts or more, using spectra with 30 bins in the energy range between 0.2 and 12 keV. To estimate the number of effective parameters we compared these χ^2 values to χ^2 distributions for different degrees of freedom, finding that the number of effective parameters is 12 for pn and 7 for MOS. As almost all background spectra have a high number of counts (see left panel of Fig. 1), the second step consists of binning the background spectra to at least 20 counts/bin and getting p-values based on the χ^2 values for this binning and the number of effective parameters estimated in the first step. For the very few cases (0.3 per cent), where we had too few counts, we

reduced the minimum number of counts per bin to 10 in the spectra of the corresponding detector. If this still gave us too few bins (0.04 per cent), we reduced the number of effective parameters until we were able to estimate a p-value and flagged the detections to exclude them from the *Good fit sample* (see Sect. 3).

A χ^2 p-value ≥ 0.01 is considered as an acceptable fit. For detections that have spectra in both detectors and where the χ^2 p-value in one detector is below that limit while it is above in the other one, only the source spectrum of the latter detector is considered.

2.2.2 Source model

As source model we used an absorbed power law model. We included the cflux model to derive the flux in the 0.2 to 12.0 keV band (cflux*TBabs*powerlaw in Xspec). In case the object is observed by both detectors, an inter-instrument normalisation constant is included. Free parameters are the logarithm of the hydrogen column density of the absorber, which is allowed to vary between 20 and 26 $\log_{10}(cm^{-2})$, the power-law photon index, which can vary between 0 and 6, the logarithm of the flux, which can vary between -7 and -17 $\log_{10}(erg\ cm^{-2}\ s^{-1})$, and the inter-instrument normalisation in all cases defined as pn/MOS that is constrained to be between 0 and 5. BXA requires the setting of a probability prior for each free parameter in the model. We used flat priors for all four parameters.

2.3 Best-fit parameters and error computation

The UltraNest algorithm implemented in BXA gives the marginalized posterior probability distribution for all free parameters in the fitted model. We used these distributions to estimate the best-fit parameters and the corresponding errors. For each free parameter we provide the median with percentiles of 5 and 95 per cent. We also provide the mode, calculated using a half sample algorithm [Robertson and Cryer, 1974] that makes use of functions from Henry Freudenriech (Hughes STX) statistics library (called ROBLIB) from AstroIDL User's Library, with the 90 per cent highest probability density interval (which corresponds to the narrowest interval that includes 90 per cent of the probability), calculated using Chen-Shao algorithm [Chen et al., 2000].

2.4 Goodness of fit

Since we have used Cash statistics for the fits and a large fraction of the spectra have less than 100 net counts, we have decided not to use χ^2 as a goodness-of-fit indicator. Cash maximum likelihood statistics lacks a direct estimate of goodness of fit (GoF). Therefore, we calculated the Kolmogorov-Smirnov (KS) statistic between two cumulative distributions, and the corresponding p-value, as a quantitative estimate of the GoF. We note however that in this case the p-values for the KS statistic cannot be calculated the usual way. The cumulative distribution of the model depends on the parameters that were estimated from the data distribution. This implies that the two compared distributions are not independent. Nevertheless, we can do a permutation test to get an estimate of the p-value. For each source, we did 1000 resamplings, rearranging the original data+model sample in two equal-size subsamples, where the counts in each energy bin can come either from the data or the model sample, and estimate the corresponding KS statistic. Our estimated p-values are the ratio of resamplings that have statistics larger than the statistic of the original samples. Any model showing a KS p-value ≥ 0.01 is considered as an acceptable fit (Fig. 2).

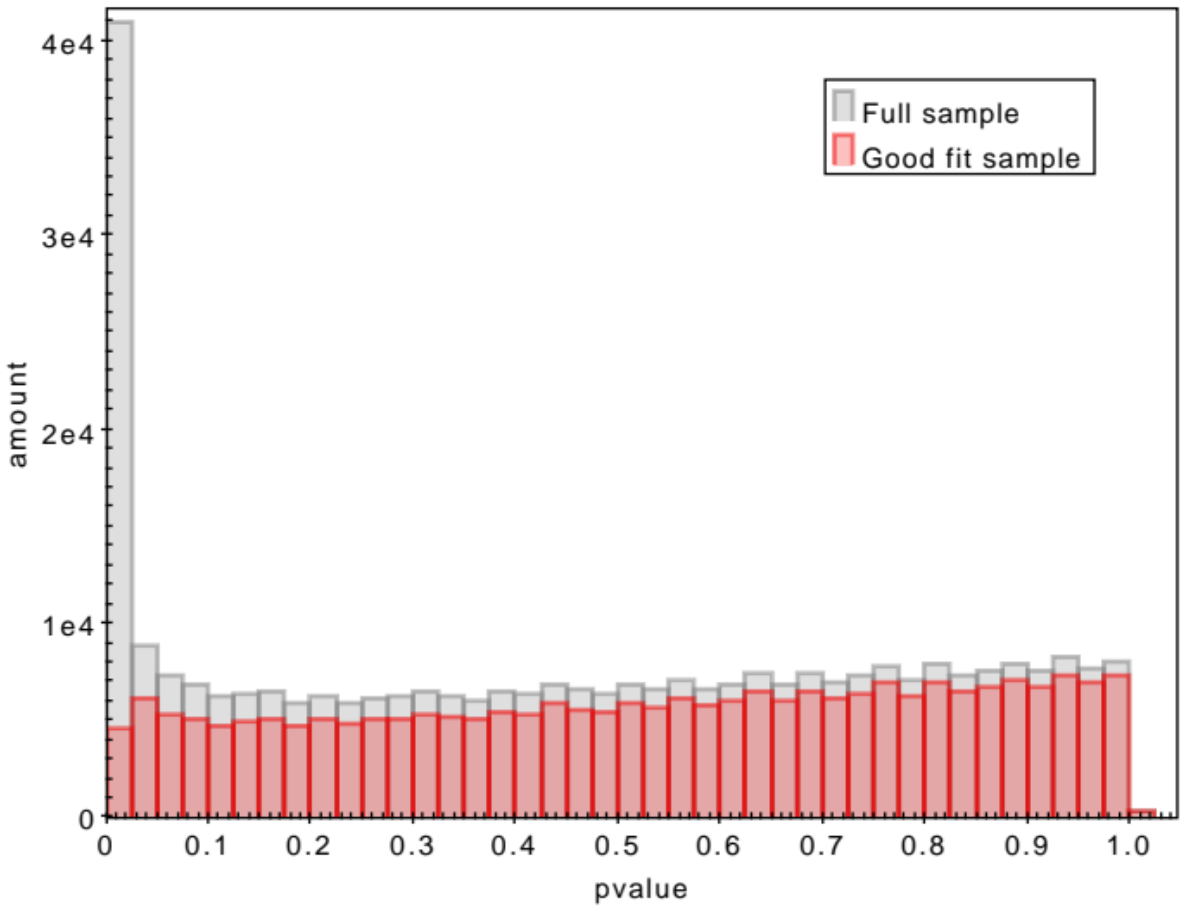

Figure 2: Distribution of the goodness-of-fit p-values for the fits to the source+background spectra.

3 Results

In total we fitted 319565 detections that have spectra in the 4XMM–DR11 catalogue. For 1621 detections (0.5 per cent) the automated definition of a background extraction region of at least one instrument [Webb et al., 2020] failed and the resulting background spectrum has no counts. If we demand that a detection has more than 0 net counts in each contributing detector (pn and/or MOS) a further 6805 detections (2.1 per cent) need to be excluded. This leaves us with a *Good sample* of 311139 detection (97.4 per cent).

Of the remaining detections, 60118 detections (18.8 per cent) gave formally unacceptable fits for the background model and a further 18575 detections for the source model (5.8 per cent). A further 96 detections (0.03 per cent) had too few counts in the background spectrum of at least one detector to obtain χ^2 p-values with the number of effective parameters being 12 for pn and 7 for MOS. Thus 232350 detections (72.7 per cent) remain within the *Good fit sample*.

Table 1: Overview of the number of detections in each sample. See Sect. 3 for the definition of the Good and Good fit samples. We call a detection low Galactic latitude if abs(BII)≤ 20, and high Galactic latitude if abs(BII)> 20.

	total	low Gal. lat.	high Gal. lat.
	319565 (100%)	117113 (36.6%)	202452 (63.4%)
Good sample	311139 (97.4%)	112504 (35.2%)	198635 (62.2%)
Good fit sample	232350 (72.7%)	69052 (21.6%)	163298 (51.1%)
Pointlike good fit sample	209634 (65.6%)	60072 (18.8%)	149562 (46.8%)

3.1 Description of the columns

Our catalogue contains one row for each detection, and 61 columns containing information about the source detection and the spectral-fitting results. Values that are not available are represented by an empty "nan" (or "null") value. The first 15 columns contain information about the source and observation, the following 24 columns contain information about the fitted model parameters (parameter values and confidence intervals), after that 7 columns provide spectral-fit statistics and flags, and the last 15 columns correspond to source detection and observation level flags taken from 4XMM-DR11.

3.1.1 Source and observation

DETID: A unique identifier, as in 4XMM–DR11.

OBS_ID: The XMM-Newton observation identification, as in 4XMM–DR11.

SRC_NUM: The (hexadecimal) source number in the individual source list for this observation (OBS ID).

RA: The right ascension, as in 4XMM–DR11.

DEC: The declination, as in 4XMM–DR11.

LII: The longitude, as in 4XMM–DR11.

BII: The latitude, as in 4XMM–DR11.

The following set of columns is given for both the pn and MOS detectors that contribute to a detection. If one of them does not contribute the values are set to "nan". "*det*" can be "pn" or "MOS".

*det*_cts: Number of total counts in the source extraction area.

*det*_bkgcts: Number of counts in the background extraction area.

*det*_netcts: Number of net counts in the source extraction area.

*det*_exp: Exposure time in seconds.

3.1.2 Model related columns

In the next 24 columns we give for each of the four free parameters the median and mode with the corresponding lower and upper boundaries. Possible parameter names are: lgflux (logarithm of the flux in the 0.2 to 12.0 keV band, in units of log 10 (erg cm^{-2} s^{-1})), logNH (logarithm of the hydrogen

column density of the absorber, in units of log 10 (cm^{-2})), PhoIndex (photon index), and IIN (inter-instrument normalisation).

PARAMETER med: Median of the parameter value.

PARAMETER med min, PARAMETER med max: Percentiles of 5 and 95 per cent.

PARAMETER mod: Mode of the parameter value.

PARAMETER mod min, PARAMETER mod max: Lower and upper limits of the 90 per cent credible interval for the parameter.

3.1.3 Fitting statistics

dof: Degrees of freedom of the source fit.

pvalue: KS p-value of the source+background fit.

pval_bkg_*det*: χ^2 p-value of the background fit for the pn and MOS detectors, if contributing. "*det*" can be "pn" or "MOS".

flag:

1: No background counts in at least one detector/camera;

2: Net counts below/equal to zero in at least one detector;

3: Formally unacceptable background fit (pval_bkg_*det* < 0.01; in case both detectors contribute, this has to be true for both of them);

4: Formally unacceptable fit (pvalue < 0.01);

5: Too few background counts to obtain χ^2 p-values with fixed number of effective parameters;

0: None of the previous issues occurred.

det_there and det_use: Two flags indicating if a detector provides a spectrum for a detection (det_there) and if it is used in the fitting (det_use). The entries are 0 for pn, 1 for MOS, and 2 for pn+MOS. In case of det_use, no entry means that both detectors are omitted.

3.1.4 Source detection parameters and flags

SUM_FLAG: Entries from the "SUM_FLAG" column, as in 4XMM–DR11.

OBS_CLASS: Entries from the "OBS_CLASS" column, as in 4XMM–DR11.

is_ext: Flag indicating if a detection is point-like (0) or extended (1), according to the "EP_EXTENT" column, as in 4XMM–DR11.

EP_EXTENT: Entries from the "EP_EXTENT" column, as in 4XMM–DR11.

mos_fast: Flag indicating if one or both MOS cameras are in the "Fast (Un)compressed" mode (1); otherwise 0

PN_MASKFRAC: Entries from the "PN_MASKFRAC" column, as in 4XMM–DR11.

M1_MASKFRAC: Entries from the “M1_MASKFRAC” column, as in 4XMM–DR11.

M2_MASKFRAC: Entries from the “M2_MASKFRAC” column, as in 4XMM–DR11.

EP_FLAG: Entries from the “EP_FLAG” column, as in 4XMM–DR11.

PN_FLAG: Entries from the “PN_FLAG” column, as in 4XMM–DR11.

M1_FLAG: Entries from the “M1_FLAG” column, as in 4XMM–DR11.

M2_FLAG: Entries from the “M2_FLAG” column, as in 4XMM–DR11.

VAR_FLAG: Entries from the “VAR_FLAG” column, as in 4XMM–DR11.

CONFUSED: Entries from the “CONFUSED” column, as in 4XMM–DR11.

HIGH_BACKGROUND: Entries from the “HIGH_BACKGROUND” column, as in 4XMM–DR11.

3.2 Fluxes

We included the cflux component in our model to obtain fluxes in the 0.2 to 12.0 keV band. In case of multiple instrument spectra for a detection, the reported flux is the pn flux. For non-extended detections of the *Good fit sample* a comparison of the mode of the logarithm of the flux derived from the spectra in the 0.2 to 12.0 keV band with the logarithm of the EP_8_FLUX (0.2 – 12.0 keV) given in the 4XMM-DR11 catalogue is shown in Fig. 3. For 86.5 per cent of these detections the flux obtained from our spectral fit agrees within errors with the flux given in the 4XMM-DR11 catalogue. For (large) extended sources, the spectrum should underestimate the flux compared to the flux reported in the catalogue, as only the latter takes the extent into account. The fluxes in the catalogue are derived from count rates obtained in five individual bands and assuming an absorbed power law model, with absorbing column density $N_H = 3.0 \times 10^{20}$ cm^{-2} and continuum spectral slope $\Gamma = 1.7$ [Webb et al., 2020]. Therefore, we also show plots of the flux-flux relation in Fig. 3, where we indicate the photon index and hydrogen column density of the absorber obtained from our fits, respectively. From these two plots it is obvious that detections that lie further away from the one-to-one correlation show a photon index or hydrogen column density that differs significantly from the one assumed in the 4XMM-DR11 catalogue. Please also remember that the fluxes from the source catalogue can include a contribution from instruments for which no spectra have been extracted.

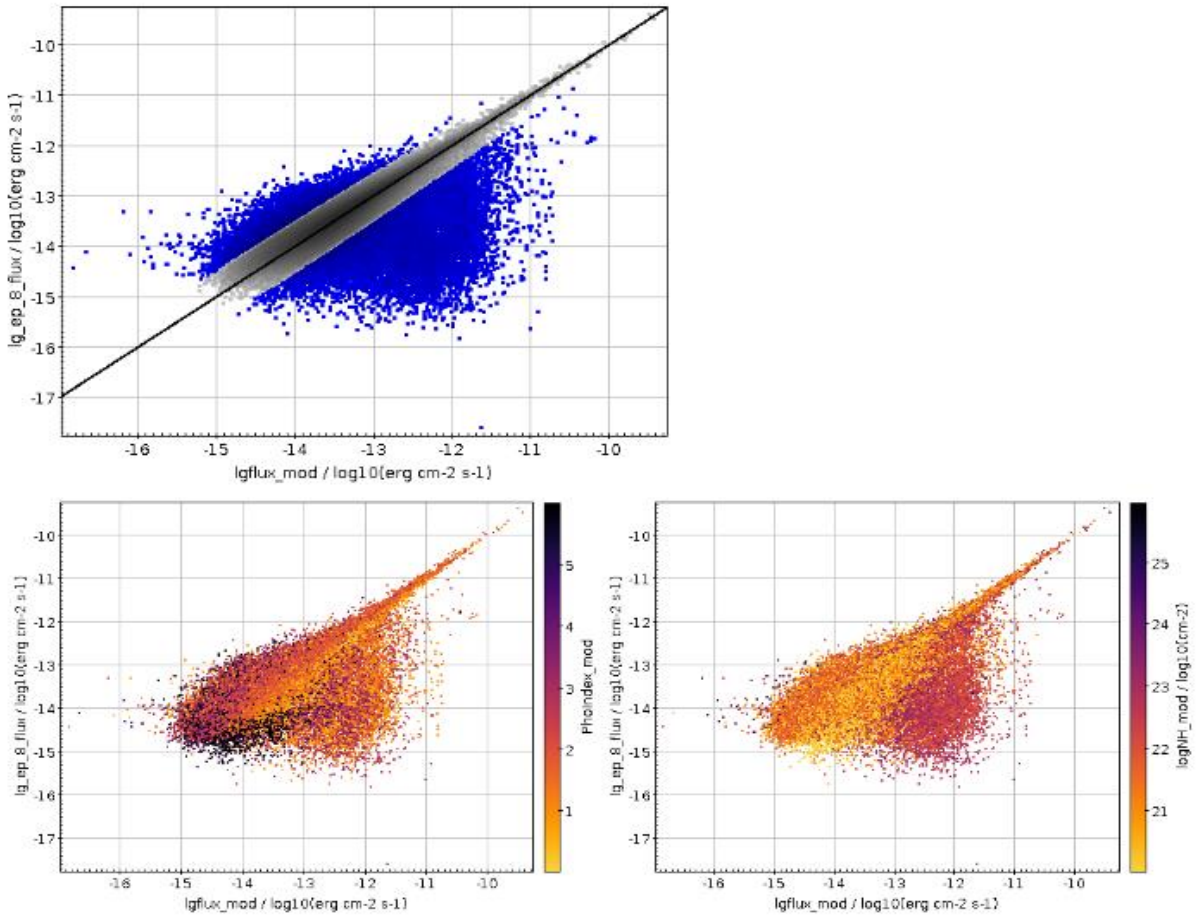

Figure 3: Distribution of the fluxes obtained from spectral fits versus fluxes from the 4XMM-DR11 catalogue for point-like detections in the Good fit sample. The grey band in the upper panel contains 90 per cent of the detections. The two lower panels indicate the hydrogen column density (left) and photon index (right) obtained from the fit, respectively.

3.3 Inter-instrument normalisation

Figure 4 (left panel) shows the distribution of the inter-instrument normalisation defined as pn over MOS. We notice that for the *Good fit sample* about 5 per cent of the detections show an inter-instrument normalisation above 2 or below 0.5 (in the following called "extreme cases"). First of all, please remember that we combined the spectra of the two MOS instruments if both are present. This merging includes cases where we combine spectra taken in two different detector submodes. Furthermore, the submodes between the pn and MOS instruments can also differ. We checked the relative contribution to the overall and the extreme cases for the different detector submode combinations. A significantly enhanced contribution to the extreme cases is only found for observations where any pn submode is combined with the "Fast (Un)compressed" mode of one or both MOS. However, this cannot explain the relative number of extreme cases, as there are only few detections (0.7 per cent of the detections in the Good fit sample that have pn and MOS spectra) with this combination of submodes.

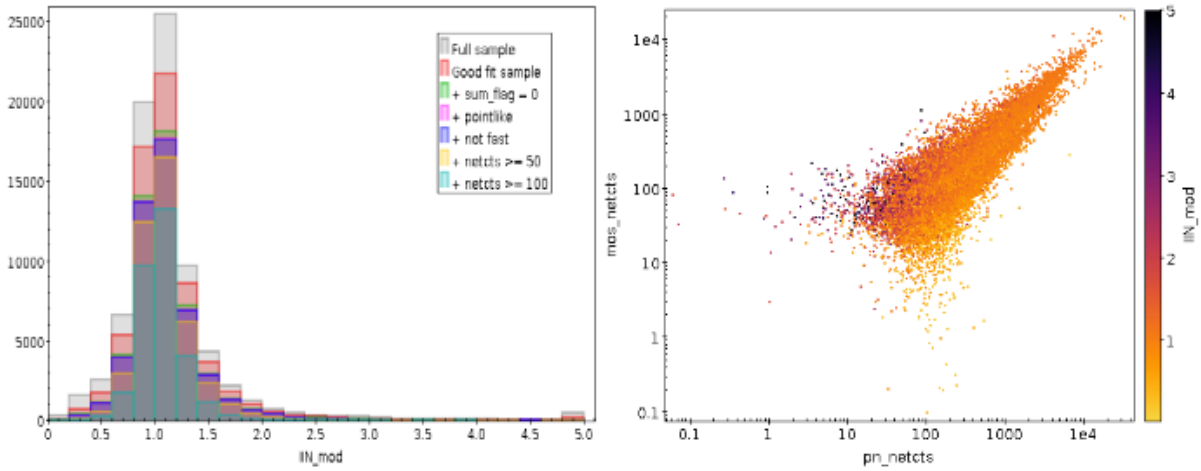

Figure 4: Distribution of the inter-instrument normalisation obtained from spectral fits applying different filters (left panel; see Table 2). The right panel shows the dependence of the inter-instrument normalisation on the net counts in the two instruments for point-like detections with flag = 0 and sum_flag =0 and excluding observation where one or both MOS are in the "Fast (Un)compressed" mode (corresponding to the blue histogram on the left-hand-side panel).

We also checked for possible effects of low or different maskfrac between pn and MOS. Spectra are only provided for detectors with a pn and MOS maskfrac ≥ 0.5. There does not seem to be a correlation between the IIN and the maskfrac difference between the two instruments.

Table 2: Number of detections in different samples for all detections that have spectra in both instruments and for those where the mode of the inter-instrument normalisation is smaller than 0.5 or bigger than 2.0. The net counts threshold is applied to both instruments individually. "not fast" means that we exclude detections where one or both MOS are in the "Fast (Un)compressed" mode.

	IIN	IIN< 0.5 or IIN>2.0
Good fit sample	63840	3604
flag = 0 + sum_flag = 0	51258	2087
flag = 0 + sum_flag = 0 + pointlike	49555	1899
flag = 0 + sum_flag = 0 + pointlike + not fast	49469	1897
flag = 0 + sum_flag = 0 + pointlike + not fast + netcts ≥ 50	42830	746
flag = 0 + sum_flag = 0 + pointlike + not fast + netcts ≥ 100	30739	198

We would like to point out that we found that there is a disproportionately high contribution of detections with sum_flag > 0 to the extreme cases, which includes possibly spurious detections. Focusing only on detections with sum_flag = 0, we find that there is a dependence of the inter-instrument normalisation on the net counts (see Fig. 4, right panel, and Table 2), with the fraction of discrepant IIN decreasing when the number of net counts increases.

3.4 Spectral parameters

For the discussion below we have cross-correlated our Good sample with the SIMBAD [Wenger et al. 2000] database, based the 4XMM-DR11s source positions and a circular area of radius 5 arcsec, using the xmatch CDS service and TOPCAT [Taylor 2005].

We show in Fig. 5 the distribution of the best fit values of the column density NH (top left) and the photon index Γ (top right). We also show NH versus Γ (bottom right): it is clear that most sources are in a vertical band around Γ~1-3, but there is a well populated "branch" of sources towards the right with a slight angle. Looking at the SIMBAD identifications (bottom right), it is clear that this branch is mostly populated by Galactic stars and galaxies. We believe that the branch is caused by trying to fit thermal emission with an absorbed power law. Most AGN are in the vertical band.

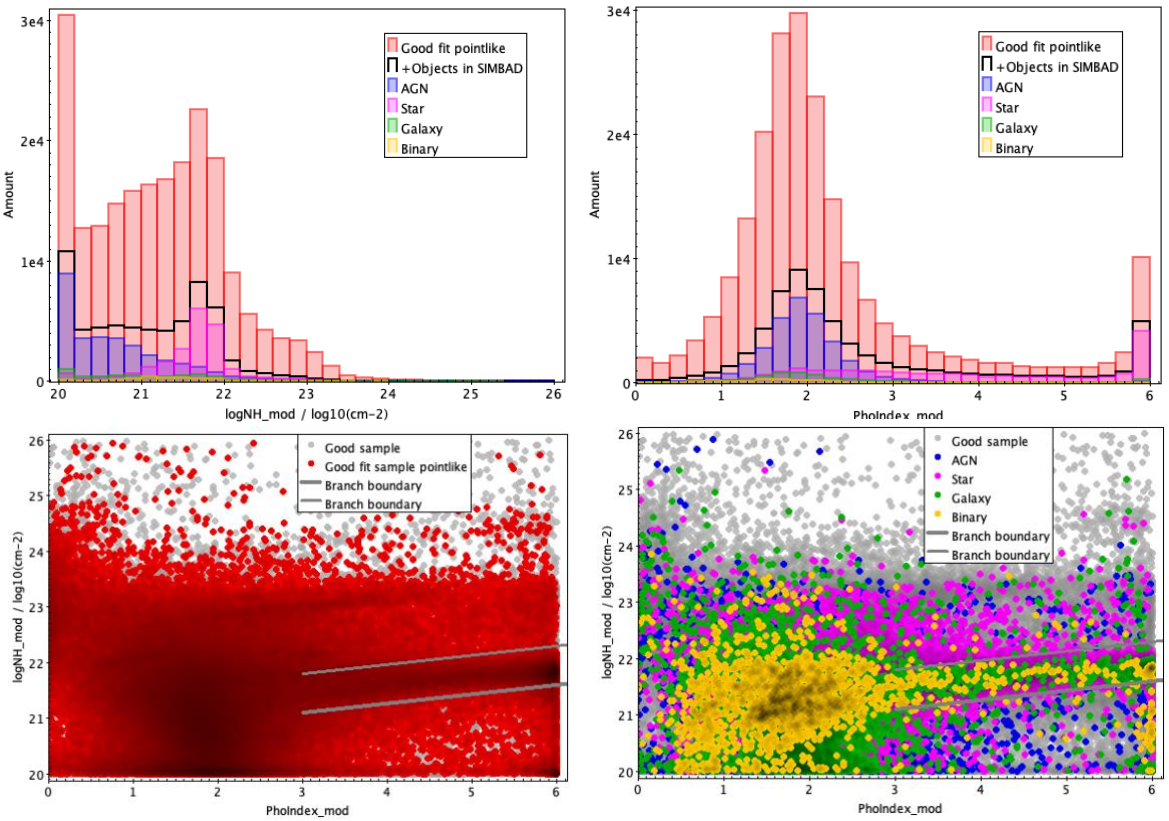

Figure 5: Distributions of the best fit values of the logarithm of the column density (logNH_mod) and the photon index (PhoIndex_mod), for the good sample and the Good fit power law sample of pointlike sources. Top left: distribution of logNH. Top right: distribution of PhoIndex. Bottom left: logNH versus PhoIndex with the "branch" delimited by grey lines (see text). Bottom right: logNH versus PhoIndex with colours for different types of sources.

Acknowledgements

This project has received funding from the European Union's Horizon 2020 research and innovation program under grant agreement n°101004168, the XMM2ATHENA project. This research has made use of the SIMBAD database, operated at CDS, Strasbourg, France. This research made use of the cross-match service provided by CDS Strasbourg.

References

J. Buchner, A. Georgakakis, K. Nandra, L. Hsu, C. Rangel, M. Brightman, A. Merloni, M. Salvato, J. Donley, and D. Kocevski. X-ray spectral modelling of the AGN obscuring region in the CDFS: Bayesian model selection and catalogue. A&A, 564:A125, Apr. 2014. doi: 10.1051/0004-6361/201322971.

M. H. Chen, Q.-M. Shao, and J. G. Ibrahim. Monte Carlo Methods in Bayesian Computation, page 387. Springer Series in Statistics. Springer, New York, NY, 2000. doi: 10.1007/978-1-4612-1276-8.

P. Freeman, S. Doe, and A. Siemiginowska. Sherpa: a mission-independent data analysis application. In J.-L. Starck and F. D. Murtagh, editors, Astronomical Data Analysis, volume 4477 of Society of Photo-Optical Instrumentation Engineers (SPIE) Conference Series, pages 76–87, Nov. 2001. doi: 10.1117/12.447161.

P. Maggi, F. Haberl, P. J. Kavanagh, S. D. Points, J. Dickel, L. M. Bozzetto, M. Sasaki, Y. H. Chu, R. A. Gruendl, M. D. Filipović, and W. Pietsch. Four new X-ray-selected supernova remnants in the Large Magellanic Cloud. A&A, 561:A76, Jan. 2014. doi: 10.1051/0004-6361/201322820.

T. Robertson and J. D. Cryer. An iterative procedure for estimating the mode. J. Am. Stat. Assoc., 69(348): 1012–1016, 1974. doi: 10.1080/01621459.1974. 10480246.

M.B. Taylor. TOPCAT & STIL: Starlink Table/VOTable Processing Software. Astronomical Data Analysis Software and Systems XIV ASP Conference Series, Vol. 347, Proceedings of the Conference held 24-27 October, 2004 in Pasadena, California, USA. Edited by P. Shopbell, M. Britton, and R. Ebert. San Francisco: Astronomical Society of the Pacific, 2005., p.29

N. A. Webb, M. Coriat, I. Traulsen, J. Ballet, C. Motch, F. J. Carrera, F. Koliopanos, J. Authier, I. De la Calle, M. T. Ceballos, E. Colomo, D. Chuard, M. Freyberg, T. Garcia, M. Kolehmainen, G. Lamer, D. Lin, P. Maggi, L. Michel, C. G. Page, M. J. Page, J. V. Perea-Calderon, F. X. Pineau, P. Rodriguez, S. R. Rosen, M. Santos Lleo, R. D. Saxton, A. Schwope, L. Tomás, M. G. Watson, and A. Zakardjian. The XMM-Newton serendipitous survey. IX. The fourth XMM-Newton serendipitous source catalogue. A&A, 641:A136, Sept. 2020. doi: 10.1051/0004-6361/201937353.

M. Wenger, F. Ochsenbein, D. Egret, P. Dubois, F. Bonnarel, S. Borde, F. Genova, G. Jasniewicz, S. Laloë, S. Lesteven, R. Monier. The SIMBAD astronomical database. The CDS reference database for astronomical objects. A&AS, 143:9, Apr. 2000. doi: 10.1051/aas:2000332